Engineering Science and Military Technologies
Volume (9) - Issue (1) - March 2025
ISSN: 2357- 0954
DOI:10.21608/EJMTC.2024.280806.1276

Original Article

Noninvasive spectral monitoring for radiation therapy induced skin-inflammation

Ramy Abdlaty[1,*], Lilian Doerwald-Munoz[2], Ahmed K. Elsherif[3], Joseph Hayward[2], Qiyin Fang[4]

Department of [1]Biomedical Engineering, [3]Engineering Mathematics, Military Technical College, Cairo, Egypt, [2]Juravinski Cancer Centre, Hamilton Health Sciences, Ontario, [4]Engineering Physics, McMaster University, Ontario, Canada.

Keywords:
Erythema, hyperspectral imaging, image classification, radiotherapy, skin.

Corresponding Author:
Ramy Abdlaty, Department of Biomedical Engineering Military Technical College, Cairo, Egypt **Tel.:** 201008319191, **Email:** ramy.elghwas@mtc.edu.eg

Abstract
In the pursuit of improving the quality of radiotherapy treatment for skin cancer, meticulous monitoring of skin toxicity is imperative. This monitoring process focuses on examining the emergence of acute skin toxicity resulting from radiation exposure. Skin toxicity is a prevalent issue affecting approximately 90% of patients undergoing ionizing radiation therapy for cancer treatment. This study explores the utility of hyperspectral imaging (HSI) in quantifying the inflammatory response of skin erythema, a common manifestation of skin toxicity. Expert visual assessment (VA), optical imaging, and HSI were employed to monitor induced skin erythema in five recruited skin cancer patients undergoing radiotherapy. Erythema indices were calculated using Dawson's formulas applied to the HSI data, and the results were compared to VA. The findings revealed a strong correlation between the computed relative erythema index and VA, indicating its potential as an objective measure. Furthermore, the study demonstrated that HSI outperforms optical imaging in accurately classifying skin erythema in precision and specificity. Thus, HSI is a promising tool for investigating toxicity symptoms associated with various dermatological conditions.

1. INTRODUCTION

Keratin-based-skin cancer (KSC) along with cutaneous melanoma (CM) are the prevalent categories of cancer in Caucasian people[1]. Skin cancer (SC) exhibited incremental incidence cases universally but steady or declining morbidity measures[2,3]. For instance, In the USA the dumping numbers of SC dead patients were recently reported[4]. This fact is probably reflecting the efficacy of proposing new systemic treatments[5].

SC is treated using multiple approaches, however, surgery and radiotherapy (RT) are more commonly exploited[6,7]. Surgery is a shortcut way for SC treatment if available and preferred[8]. Abandoning the surgery approach is probably due to possible effects on the patient's quality of life or a life-threatening reason for senior patients[9]. Therefore, the majority of elderly SC patients are referred to RT for treatment[10]. RT is not a flawless treatment approach, since it causes some undesirable side effects including radiation-based-skin toxicity[11]. Toxicity of the patient's skin is a compulsory outcome of RT on average for 90% of SC patients[12]. The toxicity severity varies from mild to harsh including the subsequent symptoms:

1- Skin inflammation (erythema) rises up after a few hours to be the most primitive skin reaction[13]. However, in rare cases, it may not become visible before 2 weeks of RT treatment[14].

2- Aching of the cutaneous epidermis that emerges as a result of the inconsistent necrosis of the skin's superficial cells after 3 weeks of radiation. The outcome of the skin aching is desquamation either being dry or moist.

3- A cutaneous ischemia and cell death probably take place within 3 months after irradiation onset[15].

4- Delayed skin destruction, telangiectasia, and harsh dermatological necrosis perhaps arise in 12 months[16].

The work reported in this study aimed to monitor RT induced skin toxicity involving erythema quantitatively. Skin erythema is an inflammatory reaction that turns the skin color into a reddish color. The red region of the skin is an expression of an impairment to the basal layer of the epidermis. This impairment leads to a vasodilation action that increases the blood content in the skin's dermal layer[17]. The content of the epidermis layer including blood nutrition lies within 2mm depth. This depth is within the penetration depth of the visible-near-infrared (VNIR) light[18]. Therefore, the scattered VNIR light out of the skin indirectly senses erythema via blood content change in the dermis.

Endeavors were exerted to exploit VNIR light in multiple techniques for evaluating changes in skin color[19]. The most dominant technique is the VA by dermatologists[20]. Although VA is dominant, it suffers from being neither quantitative nor objective[21]. Toward objective assessment, manifold techniques including diffuse reflection spectral (DRS) measurements and optical imaging, were widely investigated. The investigation results were not highly satisfying for skin healthcare givers and clinicians. They disapprove the small region of investigation provided by DRS beside its need for direct skin contact. On the other hand, clinicians criticized optical imaging for delivering poor spectral information. Thus, an intellectual approach for acquiring clinicians better satisfaction is to combine the favors of both DRS and optical imaging, and overcomes their individual downsides in a technique likewise hyperspectral imaging[22].

HSI is more than 30 years old[23], however, the favors of such technique open the research gate to be always involved in new applications[24–26]. The current and future applications of HSI in the medical field are numerous[27,28]. HSI is distinguished for capturing successive number of frames for a well-defined location. Each frame is specified by a central wavelength. In this manner, HSI overcomes DRS, optical imaging, and VA for being contactless, rich in spectral data, and objective, respectively. However, HSI loses in return the simplicity and gains lengthy time for data processing. For instance, the datacubes produced by HSI need high-speed processors to reach real-time data analysis.

This study highlights HSI as an effective, non-invasive tool for objectively assessing radiation-induced skin erythema. HSI's ability to analyze large skin areas with high sensitivity and specificity, using erythema indices and image classification, provides clear advantages over traditional optical imaging methods. The results suggest that HSI is not only accurate in detecting skin inflammation and toxicity but also holds significant potential for broader applications in skin injury monitoring.

2. MATERIALS AND METHODS

2.1. Clinical Procedure

The study's work procedure was reviewed and permitted by the responsible committee board for research ethics regarding human experiments at McMaster University, Hamilton, Ontario, Canada. The study's permission involved a requirement for patients to meet specific criteria for inclusion. Essentially, being diagnosed with SC and undergoing radiation therapy for treatment constituted the condition for being included in the study. Conversely, certain conditions led to exclusion from the research: (1) the presence of skin color patches within the treatment area, (2) the sudden appearance of erythema before receiving radiotherapy in the area of interest, (3) missing or discontinuing study sessions before or during treatment completion, and (4) using topical creams during radiotherapy without consulting the research's radiotherapist.

Adhering to these inclusion and exclusion criteria, only five patients managed to adhere to the research protocol, while three others were excluded. Table 1 contains demographic data for the compliant participants. Inadvertently, none of the consented participants had melanoma SC. The examined regions of interest (ROIs) were in distinctive body locations involving the head, upper limb, and lower limb. Entirely, the participants were referred to radiotherapy for 10 or more radiation treatment sessions. A printed permission was handed by all the participating patients in the study. The participants' median age is 75 years and 60% of them are males. A lesion on the right side of the face of one recruited patient is shown in Figure 1.

Table 1: Demographic data of the study's participants

Patient #	Gender/ Age	Region of interest	# of sessions
1	Female/ 88	Tibia	20
2	Female/ 56	forearm	20
3	Male/ 68	Cheek	10
4	Male/ 85	Ear	10
5	Male/ 75	Temple	10

Fig. 1: Digital color images montage for a facial skin cancer patient. The sequence of images displays the development of skin toxicity (erythema) symptoms. The images were arranged from left to right and from up to down chronically. The patient had originally no trace of skin redness before the onset of radiotherapy. Once he started radiation sessions, erythema rises up gradually to express the skin toxicity.

2.2. Visual assessment

Day-to-day, the patient meets our study's radiotherapist to verbally answer a simple questionnaire regarding his/her activity the day before. The main purpose of that verbal speech is to record any side effects of RT especially skin symptoms. All the recorded information along with the radiotherapist observations for skin status are saved both on paper and digital files for each patient. Skin-erythema observations were ranked on a 5-phases measure[29,30] as shown in Figure 2. Each phase of the measure is mapped to a percentage score.

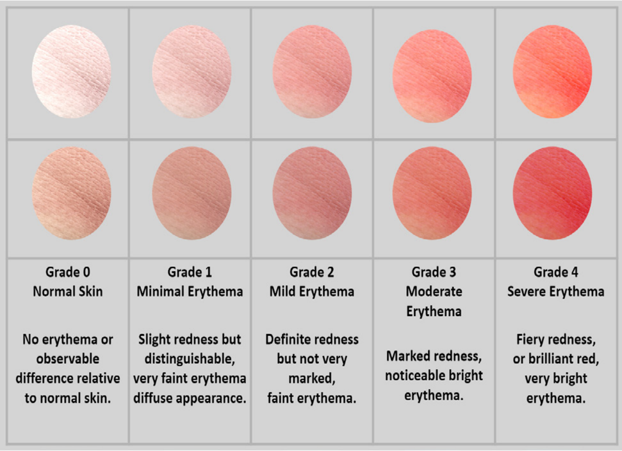

Fig. 2: displays the radiotherapist erythema assessment measure developed specifically for reference use in the field of radiation therapy. The measure encompasses a group of reference skin photographs resembling each phase of skin redness color taking into consideration 2 varying shades of Caucasian skin.

2.3. Optical Imaging

The patients' lesion ROI is pictured daily using a color camera. The daily picture records the health status of the patient's ROI along the non-irradiated skin region. The non-irradiated region facilitated the keeping of a record of the status of the normal skin. Besides, color images provided the chance to perform an authentication of the erythema VA measures given by the other non-attending radiotherapists.

2.4. Hyperspectral imaging

The HSI hardware utilized in this study was custom-designed and developed by our research team. It underwent testing on skin-simulating phantoms and examination on artificially induced skin erythema to measure changes in tissue composition[31]. In brief, our in-house HSI optical setup incorporates dual halogen illumination emitters to illuminate the ROI within the tissue. The backscattered photons are then collected by a series of optical components and directed toward an acousto-optic tunable filter (AOTF) crystal (TF625-350-2-11-BR1A, Gooch & Housego, Cleveland, OH, USA) device. This device separates the spectral range into narrow bands. Each spectral band is sequentially transmitted to a monochromatic CMOS camera (2048 × 2048, 5.5 µm pixel size, MQ042RG-CM, Xemia, Munster, Germany) for image capture as shown in Figure 3[32].

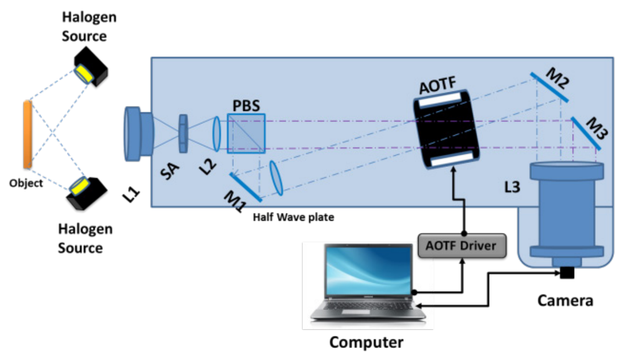

Fig. 3: A schematic drawing displays the configuration of the acousto-optic tunable filter (AOTF)-based hyperspectral imaging (HSI) system. L1: zoom lens; SA: square aperture acting as field aperture; L2, L3: achromatic lenses; M1, M2, M3: flat mirrors; PBS: polarizing beam splitter; AOTF: acousto-optic tunable filter; camera for capturing images, and computer for system control and data storage, all the components are tightly fixed to a metal platform to ensure portability.

This process is repeated three times during each session of the study for each patient: first for camera dark current, followed by a second set for a high-reflectance white surface, and finally for the patient's ROI. Each dataset comprises eighty-nine frames spanning the spectrum from 450 to 850nm and takes approximately 89 seconds to record. A schematic diagram outlining the procedure for capturing patient datasets is presented in Figure 3.

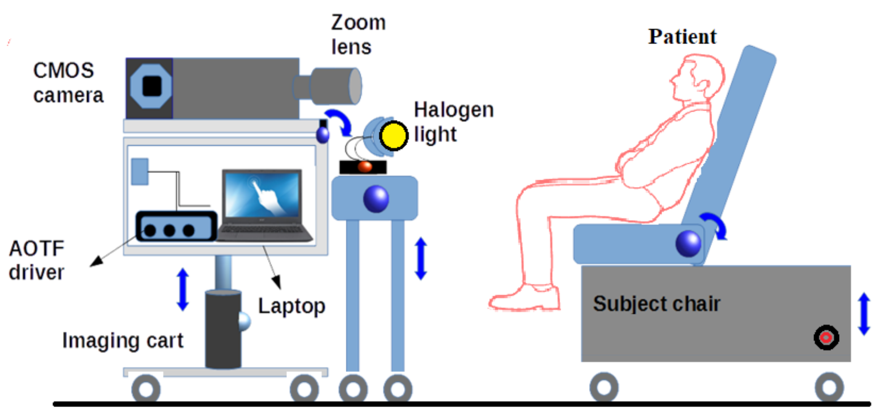

Fig. 4: A schematic diagram displaying a skin cancer patient who is accommodated for the purpose of adjusting his position for the HSI session. In this position, the human ROI is within the upper section of the body. The ROI is lightened from two directions. In case of a facial ROI, dark protection glasses are given to the patient to protect his eyes against direct light.

3. ANALYSIS OF DATA

The recorded information for each participant including, the radiotherapist daily scores for the radiation induced erythema, the optical images for the participants' ROI, and the spectral datasets were archived and labeled by date to facilitate analysis of data.

3.1. Erythema Visual Scores

The erythema score (ES) is calculated by summing the result of multiplying the radiotherapist visual erythema level (L), based on the erythema measure shown in Figure 2, and its relevant occupied region area (R) within the patient's ROI, as shown in equation 1.

$$E_S = \sum_{i=1}^{4} L_i * R_i \tag{1}$$

3.2. Spectral Reflectance Computation

A single group of raw images for the ROI along the operating spectral range is tagged a datacube. Spectral datacubes encompasses a continuous 2-dimensional images for the ROI, yet, each is recorded at a consequent spectral band. The study participants' datacubes are initially prepared for analysis. The preparation process goes across two steps. First, the dark current pixel intensities ($\boldsymbol{I}_{\text{dark}}$) are eliminated from the ROI pixel intensities ($\boldsymbol{I}_{\text{ROI}}$) by a matrix subtraction. Second, the ROI datacube is required to be neutralized for the effect of asymmetrically distributed illumination. The compensation step is accomplished by normalizing $\boldsymbol{I}_{\text{ROI}}$ to a relative pixel intensity for a white standard reflectance object ($\boldsymbol{I}_{\text{ws}}$). The precise compensation process entails sustaining the same settings of imaging for both patient's ROI and the white object. Therefore, the patient's ROI reflectance ($\boldsymbol{I}_{\text{ROI}}$) is computed as displayed in equation 2.

$$R_{ROI} = \frac{I_{ROI} - I_{dark}}{I_{ws} - I_{dark}} \tag{2}$$

3.3 Calculation of Erythema Index

The calculated erythema index is based on Dawson technique[33]. The principal of Dawson's formula is simply calculating the region enclosed confined by the curve of the inverse logarithmic value of the patients' computed reflectance in the eye-detected spectra (510-610nm) using equation 3:

$$DEI = 100 * \left[c + \frac{3}{2}(b + d) - 2(a + e)\right] \tag{3}$$

Where a, b, c, d, and e refers to the resultant number of log10 ($\boldsymbol{P}_{\text{ROI}}$) at the following selected spectral bands centered at: 510, 540, 560, 580, and 610nm, correspondingly.

3.4. Image Classification

For image classification purposes, linear discriminant analysis (LDA) technique is selected for the current study[34]. The reason for this selection is that LDA can be easily implemented for both color and spectral images. LDA implementation becomes optimal once the dependent variable, skin erythema, is represented as a categorical one provided that the independent variable is consecutive in its form likewise time plan for SC treatment. The data classes are separated by selecting the optimal plane that leads to the maximum separation between the mean for each data class provided that the divergence between the individual class members is minimal. The guiding principle of LDA is to maximize the separation between the mean centers of distinct classes while minimizing the variance within each class. The key challenge lies in identifying the optimal axis that projects the data in a manner that forms well-separated clusters. For example, the plane of optimal separation should maximize the distinction between classes, ensuring the most effective class separation. An exhibition of the chief principle of the Fisher LDA technique for data classification is shown in Figure 4.

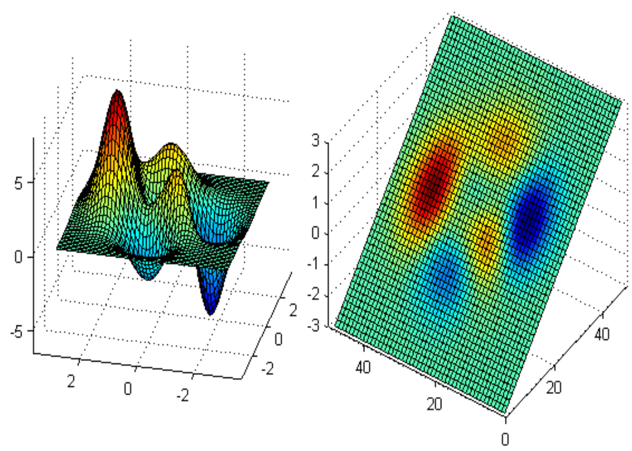

Fig. 5: displays Fisher linear discriminant analysis that classify data into separate classes by finding the optimal plane to reach the best separation between the different classes.

4. RESULTS

4.1. Visual assessment

Figure 6 displays the average scores for the computed VA regarding the skin erythema status for the participating patients. The represented data shows the mean value of the 5 patients when they complete the corresponding ratio of their treatment sessions. The error bars are representing the standard error.

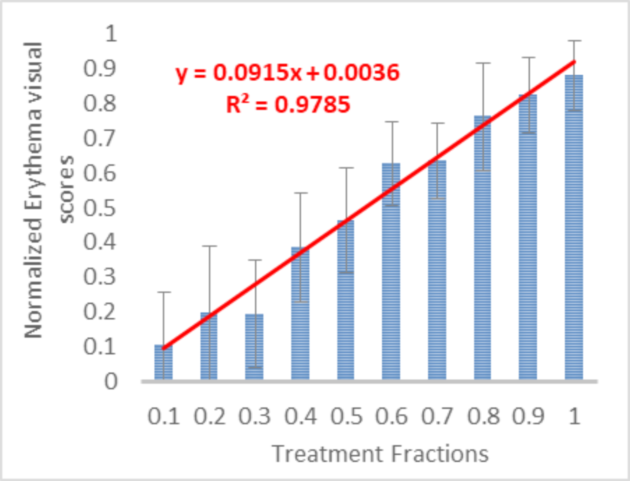

Fig. 6: illustrates the recorded normalized the mean values for the computed VA regarding the skin erythema status for the participating patients. The recorded scores are plotted against the treatment fractions. The error bars are used to show the standard error for the computed VA scores. The red trend line shows an arising skin erythema score with a squared error (R2 =0.9785).

4.2 Skin Erythema Indices

The calculated normalized melanin- corrected erythema index is illustrated in Figure 7 while the relevant relative erythema index is exhibited in Figure 8 for the recruited patients.

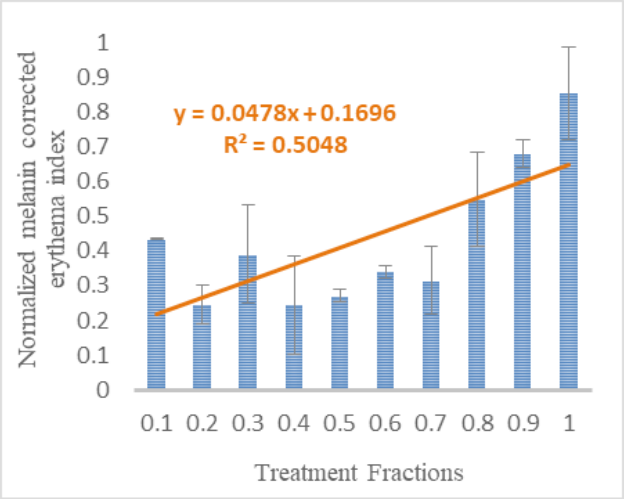

Fig. 7: displays the calculated mean value for the melanin-altered erythema index. The error bars demonstrate the variation in the figured erythema among individuals in terms of standard error. The orange trend line shows an arising skin erythema score with a squared error (R2 =0.5048).

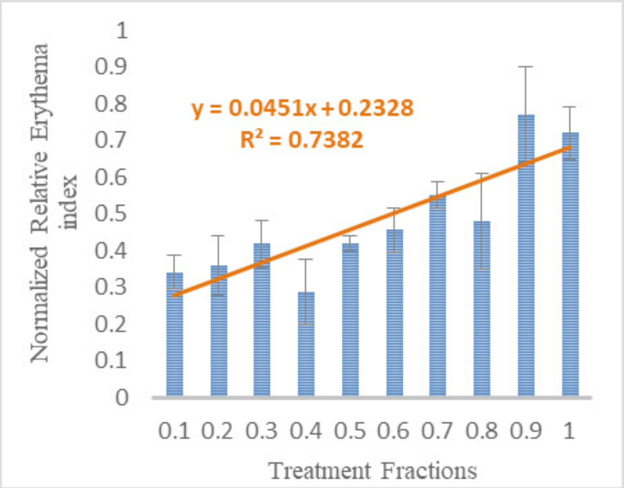

Fig. 8: displays the calculated mean value for the relative erythema calculated index. The error bars demonstrate the change in the figured index among skin cancer patients in terms of standard error. The orange trend line shows an arising skin erythema score with a squared error (R2 =0.7382).

4.3 Image classification

The adopted LDA classification technique was applied on the captured images either being spectral or color ones. The reason, for applying LDA, is to compare the two imaging modalities. HSI shows a comparable performance with traditional optical imaging in both accuracy and sensitivity. Nevertheless, HSI significantly outstrips optical imaging in not only the specificity but also in the geometrical mean. We display 6 classification parameters for spectral and optical imaging in the process of evaluating skin erythema for RT-treated SC patients in Figure 9.

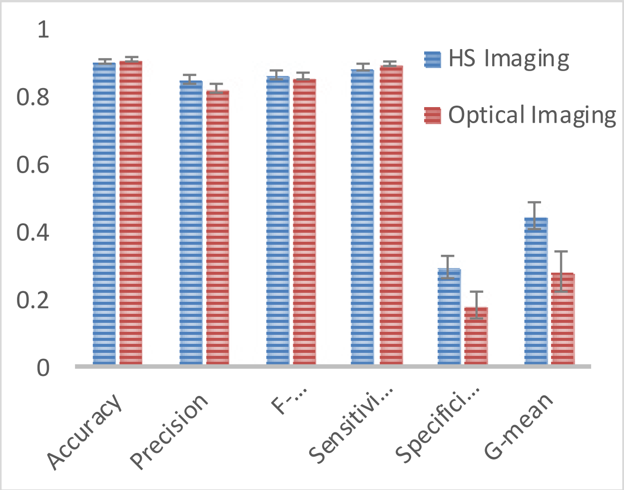

Fig. 9: displays the classification computed parameters for comparing HSI and optical imaging regarding quantifying radiation-induced skin erythema.

5. DISCUSSION

VA is the standard monitoring technique for radiation therapy toxicity. However, it is subjective, eye acuity dependent, and exposed to inter/ intra variability between the performing radiotherapists. To be unbiased toward the study's results, two alternative radiotherapists were involved in the research study. Each study session is attended by one radiotherapist while the other one performs the assessment offline based on an RGB image of the participant daily. Both participating radiotherapists are interchanged between online and offline assessments of patients. In our study, VA displayed an arising score for skin erythema along the timeline of treatment.

The computed skin erythema indices are computed based on objective daily measurements of skin spectral profile. The melanin-altered erythema index achieved less successful objective monitoring for the skin subjected to inflammation as shown in Figure 6. However, the relative erythema calculated index was more successful in following up the increase/ spread of skin erythema in proportion to the accumulation of the radiation dose as exhibited in Figure 7. The coefficient of determination in both cases of erythema indices proved that the relative erythema index is better in objectively monitoring skin inflammation. Being objective, less time consuming, in addition to lower expenses of relative erythema index makes it a potential economic skin assessment alternative.

HSI classification data presented a piece of evidence that it is performing better than traditional digital color images for dermatological inflammation[27,35]. However, the utilized HSI hardware in this study costs more than traditional digital color imaging, and technology is offering cheaper HSI solutions[36]. Moreover, the optimal distinguishing spectral bands selection procedure paves the way to replace sophisticated HSI hardware with multispectral imaging that costs less in time, money, and expertise[37].

6. CONCLUSION

This study offers a potential approach, HSI, for objective assessment of radiation-induced skin erythema. The advantage of HSI is that it provides a contactless opportunity for investigating the toxicity symptoms of radiation in a sizable skin region. We summarize the outcomes of the current work as follows:

1- The calculated relative index for RT-induced erythema is a highly sensitive parameter to sense skin inflammation.

2- The supervised image classification using the LDA method demonstrated the potency of HSI in contrast to optical imaging in specificity along with geometric mean.

3- HSI is a potentially useful technique for skin burn investigation since it is contactless, objective, and capable of studying relatively wide regions at the same time.

The progress in developing even illumination sources with less emitted heat, widely operating tunable filters, and highly sensitive while being handy camera sensors will empower HSI to be on the shelf for dermatologists' clinics. Furthermore, HSI is a good proposal for fast recognition of injuries due to working in hazardous radiation facilities. Yet, endeavor work needs to be done in both the laboratory and the clinic to authorize HSI to be a commercial instrument in dermatology clinics.

7. REFERENCES

[1] Y. Zhang, M. K. Markey, and J. W. Tunnell, "Physiological basis for noninvasive skin cancer diagnosis using diffuse reflectance spectroscopy," Photonics Dermatology Plast. Surg., vol. 10037, p. 1003707, 2017.
[2] NIH National Cancer Institute, "Cancer Facts & Figures 2020," 2020.
[3] C. Y. Wright, D. Jean du Preez, D. A. Millar, and M. Norval, "The epidemiology of skin cancer and public health strategies for its prevention in southern Africa," Int. J. Environ. Res. Public Health, vol. 17, no. 3, 2020.
[4] R. L. Siegel, K. D. Miller, H. E. Fuchs, and A. Jemal, "Cancer statistics, 2022," CA. Cancer J. Clin., vol. 72, no. 1, pp. 7–33, 2022.
[5] N. Saleh, M. A. Hassan, and A. M. Salaheldin, "Skin cancer classification based on an optimized convolutional neural network and multicriteria decision-making," Sci. Rep., vol. 14, no. 1, pp. 1–19, 2024.
[6] A. Rembielak, A. J. Sykes, K. Fife, A. Challapalli, and J. P. Nobes, "Radiotherapy and Systemic Treatment for Non-melanoma Skin Cancer in the COVID-19 Pandemic," Clin. Oncol., vol. 32, no. 7, pp. 417–419, 2020.
[7] K. Mosterd *et al*., "Surgical excision versus Mohs' micrographic surgery for primary and recurrent basal-cell carcinoma of the face: a prospective randomised controlled trial with 5-years' follow-up.," Lancet. Oncol., vol. 9, no. 12, pp. 1149–56, 2008.
[8] R. Abdlaty, L. Doerwald-munoz, T. J. Farrell, J. E. Hayward, and Q. Fang, "Hyperspectral imaging assessment for radiotherapy induced skin-erythema : Pilot study," Photodiagnosis Photodyn. Ther., vol. 33, no. January, p. 102195, 2021.
[9] S. Kumar, E. Juresic, M. Barton, and J. Shafiq, "Management of skin toxicity during radiation therapy: A review of the evidence," J. Med. Imaging Radiat. Oncol., vol. 54, no. 3, pp. 264–279, 2010.
[10] E. Yosefof, N. Kurman, and D. Yaniv, "The Role of Radiation Therapy in the Treatment of Non-Melanoma Skin Cancer," Cancers (Basel)., vol. 15, no. 9, 2023.
[11] A. Montero *et al*., "Acute skin toxicity of ultra-hypofractionated whole breast radiotherapy with simultaneous integrated boost for early breast cancer," Clin. Transl. Radiat. Oncol., vol. 41, no. May, pp. 1–7, 2023.
[12] R. M. Y. M. Abdlaty, L. Doerwald, J. Hayward, and Q. Fang, "Spectral assessment of radiation therapy-induced skin erythema," vol. 1131619, no. March, p. 43, 2020.
[13] R. Abdlaty, J. Hayward, T. Farrell, and Q. Fang, "Skin erythema and pigmentation : a review of optical assessment techniques," Photodiagnosis Photodyn. Ther., vol. 33, p. 102127, 2020.
[14] D. L. Glennie, J. E. Hayward, D. E. Mckee, and T. J. Farrell, "Inexpensive diffuse reflectance spectroscopy system for measuring changes in tissue optical properties," J. Biomed. Opt., vol. 19, no. December, pp. 105005-1-105005–6, 2014.
[15] S. Zhang *et al*., "Multimodal imaging of cutaneous wound tissue," J. Biomed. Opt., vol. 20, no. 1, pp. 016016–016016, 2015.
[16] S. Schalka, "New data on hyperpigmentation disorders," J. Eur. Acad. Dermatology Venereol., vol. 31, pp. 18–21, 2017.
[17] A. Raina, R. Hennessy, M. Rains, J. Allred, D. Diven, and M. K. Markey, "Objective measurement of erythema in psoriasis using digital color photography with color calibration," Ski. Res. Technol., no. 7, pp. 1–6, 2015.
[18] M. A. Calin and S. V. Parasca, "Automatic detection of basal cell carcinoma by hyperspectral imaging," J. Biophotonics, no. July, pp. 1–8, 2021.
[19] A. R. Matias, M. Ferreira, P. Costa, and P. Neto, "Skin colour, skin redness and melanin biometric measurements: Comparison study between Antera-3D, Mexameter and Colorimeter," Ski. Res. Technol., pp. 346–362, 2015.
[20] S. Taylor, W. Westerhof, S. Im, and J. Lim, "Noninvasive techniques for the evaluation of skin color," J. Am. Acad. Dermatol., vol. 54, no. 5, pp. S282–S290, 2006.
[21] R. Abdlaty, L. Doerwald, and J. Hayward, "Radiation Therapy Induced-Erythema : Comparison of Diffuse Reflectance Spectroscopy Measurements and Visual Assessment," in Image Perception, Observer

Performance, and Technology Assessment, SPIE Medical Imaging, 2019, no. March.
[22] L. A. Courtenay *et al*., "Hyperspectral imaging and robust statistics in non-melanoma skin cancer analysis," Biomed. Opt. Express, vol. 12, no. 8, p. 5107, 2021.
[23] B. N. R. A.F.H.Goetz, J.E. Solomon, "Imaging spectrometry for earth remote sensing," Science (80-.)., vol. 228, p. 11471153, 1985.
[24] R. Abdlaty, M. Gobara, I. Naiem, and M. Mokhtar, "Innovative technique for analysis of wastewater contaminants using hyperspectral imaging," J. Spectr. Imaging, vol. 9, pp. 1–10, 2020.
[25] D. Nishijima, M. I. Patino, and R. P. Doerner, "New application of hyperspectral imaging to steady-state plasma observations New application of hyperspectral imaging to steady-state plasma observations," Rev. Sci. Instrum., vol. 083501, no. August, 2020.
[26] M. Al Ktash, M. Stefanakis, B. Boldrini, and E. Ostertag, "Characterization of Pharmaceutical Tablets Using UV Hyperspectral Imaging as a Rapid In-Line Analysis Tool," no. June, 2021.
[27] H. Y. Huang, Y. P. Hsiao, A. Mukundan, Y. M. Tsao, W. Y. Chang, and H. C. Wang, "Classification of Skin Cancer Using Novel Hyperspectral Imaging Engineering via YOLOv5," J. Clin. Med., vol. 12, no. 3, 2023.
[28] H. Y. Huang *et al*., "A Review of Recent Advances in Computer-Aided Detection Methods Using Hyperspectral Imaging Engineering to Detect Skin Cancer," Cancers (Basel)., vol. 15, no. 23, 2023.
[29] Y. Manchanda, S. Das, A. Sarda, and P. Biswas, "Clinician Severity Assessment Grading Scale on Erythematotelangiectatic Rosacea," Indian J. Dermatol., vol. 66, no. 2, pp. 203–205, 2021.
[30] R. Yang, C. Liu, W. Liu, J. Luo, S. Cheng, and X. Mu, "Botulinum Toxin A Alleviates Persistent Erythema and Flushing in Patients with Erythema Telangiectasia Rosacea," Dermatol. Ther. (Heidelb)., vol. 12, no. 10, pp. 2285–2294, 2022.
[31] R. Abdlaty *et al*., "Hyperspectral Imaging and Classification for Grading Skin Erythema," Front. Phys., vol. 6, no. August, pp. 1–10, 2018.
[32] P. Pandey, Y. Ge, V. Stoerger, and J. C. Schnable, "High Throughput In vivo Analysis of Plant Leaf Chemical Properties Using Hyperspectral Imaging," vol. 8, no. August, pp. 1–12, 2017.
[33] J. B. Dawson *et al*., "A theoretical and experimental study of light absorption and scattering by in vivo skin.," Phys. Med. Biol., vol. 25, no. 4, pp. 695–709, 1980.
[34] N. Ganesh, S. Jayalakshmi, R. C. Narayanan, M. Mahdal, H. M. Zawbaa, and A. W. Mohamed, "Gated Deep Reinforcement Learning With Red Deer Optimization for Medical Image Classification," IEEE Access, vol. 11, no. May, pp. 58982–58993, 2023.
[35] M. B. Stuart *et al*., "Low-cost hyperspectral imaging with a smartphone," J. Imaging, vol. 7, no. 8, pp. 1–13, 2021.
[36] M. B. Stuart *et al*., "Low-cost hyperspectral imaging system: Design and testing for laboratory-based environmental applications," Sensors (Switzerland), vol. 20, no. 11, pp. 1–13, 2020.
[37] M. A. Ilișanu, F. Moldoveanu, and A. Moldoveanu, "Multispectral Imaging for Skin Diseases Assessment-State of the Art and Perspectives," Sensors, vol. 23, no. 8, 2023.